AIAA-81-1259

Numerical Solutions of the Euler Equations by Finite Volume Methods Using Runge-Kutta Time-Stepping Schemes

A. Jameson, Princeton University, Princeton, NJ; and
W. Schmidt, Dornier GmbH, Friedrichshafen, FRG; and
E. Turkel, University of Tel Aviv, Israel

AIAA 14th Fluid and Plasma Dynamics Conference

June 23-25, 1981/Palo Alto, California

NUMERICAL SOLUTION OF THE EULER EQUATIONS BY FINITE VOLUME METHODS USING RUNGE KUTTA TIME STEPPING SCHEMES

A. Jameson*
Department of Mechanical and Aerospace Engineering
Princeton University
Princeton. N.J. 08544

Wolfgang Schmidt†
Dornier GmbH
Friedrichshafen, W. Germany

Eli Turkel**
University of Tel Aviv
Tel Aviv. Israel

Abstract

A new combination of a finite volume discretization in conjunction with carefully designed dissipative terms of third order, and a Runge Kutta time stepping scheme, is shown to yield an effective method for solving the Euler equations in arbitrary geometric domains. The method has been used to determine the steady transonic flow past an airfoil using an O mesh. Convergence to a steady state is accelerated by the use of a variable time step determined by the local Courant member, and the introduction of a forcing term proportional to the difference between the local total enthalpy and its free stream value.

1. Introduction

While potential flow solutions have proved extremely useful for predicting transonic flows with shock waves of moderate strength[1], typical of cruising flight of long range transport aircraft, the approximation of ignoring entropy changes and vorticity production cannot be expected to give acceptable accuracy when the flight speed is increased into the upper transonic range. There also appears to be some disturbing discrepancies between conservative potential flow solutions and solutions of the Euler equations at quite moderate Mach numbers, such as the NACA 0012 airfoil at Mach .8 and an angle of attack of 1.25°[2] (possibly related to the existence of non-unique solutions of the transonic potential flow equation[3]).

The purpose of the present work is to develop economical methods of solving the Euler equations, particularly for steady flows, with the aim of reducing the computational cost to the point where they might be used as an alternative to potential flow calculations for design work. Since it is desired that the methods should be applicable to complex geometric configurations, the finite volume formulation has been used to develop the space discretization, allowing the use of an arbitrary grid. This has the additional advantage that calculations can be performed on the same grids as have been used for potential flow calculations, so that errors due to the potential flow assumption can be assessed.

The research stems from a visit by the first author to the Dornier company in August 1980. At that time he substituted an alternative difference scheme into a code for solving the Euler equations which had been previously developed by Rizzi and Schmidt[4]. The new method retained the finite volume formulation of the earlier method, but replaced the MacCormack scheme by a three state iterated central difference scheme for advancing the solution at each time step, comparable to the schemes of Gary[5] and Stetter[6]. A key feature was the introduction of dissipative terms in a separate filter stage at the end of each time step. The magnitude of the dissipative terms was adapted to the local properties of the flow by means of a sensor based on the local pressure gradient.

The revised method was found to offer significant advantages over the MacCormack scheme. In particular the results of a linear stability analysis indicates that the scheme is stable for Courant numbers up to 2 in one dimensional problems, and that stability is maintained in multidimensional problems with an appropriately reduced time step, without any need for splitting. These properties have been confirmed in practice, and the scheme has been found in fact to be stable enough to allow a variable time step at the limit set by the local Courant number to be used throughout computational domains with very large variations in cell size. This permits steady states to be reached in a few hundred time steps even on O meshes, where the largest cells are many million times the size of the smallest cells clustered at the trailing edge. The scheme also has the advantage that by using central differences it treats the flow on the upper and lower sides of the airfoil symmetrically on O and C meshes. whereas the MacCormack scheme requires logic to preserve the same sequence of upwind and downwind differencing on the two sides of the airfoil.

The implementation of the three stage central difference scheme for three dimensional flows has been carried out by Rizzi and is described in a separate paper[7]. In a concurrent effort the present authors have continued an investigation of alternative two dimensional schemes with the objective of finding answers to some of the following questions:

(1) What is the most efficient time stepping scheme?
(2) What is the optimal form of the dissipative terms?

---

* Professor
** Professor
† Chief of Theoretical Aerodynamics

(3) khat is the best uay to treat the boundary conditions at the body and in the far field?
(4) How can convergence to a steady state be accelerated?

It is concluded

(1) that a fourth order Runge Kutta time stepping scheme is preferable to the three stage scheme.
(2) that the dissipative terms should be constructed from an adaptive blend of second and fourth differences.
(3) that the treatment of the boundary conditions in the far field should be based on the appropriate characteristic combinations of variables.
(4) that convergence to a steady state is significantly accelerated
   (a) by using a variable time step at the maximum limit set by the local Courant number
   (b) by adding a forcing term based on the difference between the local total enthalpy and its free stream value (this implies that the energy equation must be integrated in time, and not eliminated in favor of the steady state condition that the total enthalpy is constant, as has been the practice in a number of recent applications [4,7,8]).

Some numerical results supporting these conclusions are presented in the last section. Applications of the method to practical aerodynamic problems are discussed in a companion paper, which addresses questions such as the inclusion of boundary layer corrections, treatment of the Kutta condition, and differences between potential flow and Euler solutions[9].

2. Finite Volume Scheme

Let p, ρ, u, v, E and H denote the pressure, density, Cartesian velocity components, total energy and total enthalpy. For a perfect gas

$$E = \frac{p}{(\gamma-1)\rho} + \frac{1}{2}(u^2+v^2), \quad H = E + \frac{p}{\rho} \tag{1}$$

where γ is the ratio of specific heats. The Euler equations for two dimensional inviscid flow can be written in integral form for a region Ω with boundary ∂Ω as

$$\frac{\partial}{\partial t}\iint_{\Omega} w\,dx\,dy + \oint_{\partial\Omega} (f\,dy - g\,dx) = 0 \tag{2}$$

where x and y are Cartesian coordinates and

$$w = \begin{pmatrix} \rho \\ \rho u \\ \rho v \\ \rho E \end{pmatrix}, \quad f = \begin{pmatrix} \rho u \\ \rho u^2+p \\ \rho uv \\ \rho uH \end{pmatrix}, \quad g = \begin{pmatrix} \rho v \\ \rho vu \\ \rho v^2+p \\ \rho vH \end{pmatrix} \tag{3}$$

The discretization procedure follows the method of lines in decoupling the approximation of the spatial and Temporal terms. The computational domain is divided into quadrilateral cells as in the sketch, and a system of ordinary differential equations is obtained by applying equation (2) to each cell separately. The resulting equations can then be solved by several alternative time stepping schemes.

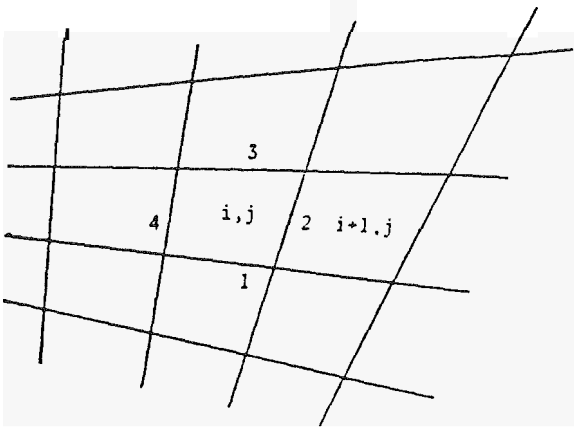

Let the values of the quantities associated with each cell be denoted by i,j. (These can be regarded as values at the cell center, or average values for the cell). For each cell equation (2) assumes the form

$$\frac{d}{dt}(hw) + Qw = 0 \tag{4}$$

where h is the cell area, and the operator Q represents an approximation to the boundary integral defined by the second term of (2). This is defined as follows. Let Δx_k and Δy_k be the increments of x and y along side k of the cell, with appropriate signs. Then the flux balance for, say, the x momentum component, is represented as

$$\frac{\partial}{\partial t}(h\rho) + \sum_{k=1}^{4} (Q_k\,\rho u_k + \Delta y_k p_k) = 0 \tag{5}$$

where h is the cell area, Q_k is the flux velocity

$$Q_k = \Delta y_k u_k - \Delta x_k v_k \tag{6}$$

and the sum is over the four sides of the cell. Each quantity such as u_1 or $(\rho u)_1$ is evaluated as the average of the values in the cells on the two sides of the face,

$$(\rho u)_1 = \frac{1}{2}(\rho u)_{i,j} + \frac{1}{2}(\rho u)_{i+1,j} \tag{7}$$

for example. The scheme reduces to a central difference scheme on a Cartesian grid, and is second order accurate provided that the grid is smooth enough.

3. Dissipative Terms

To suppress the tendency for odd and even point decoupling, and to prevent the appearance of wiggles in regions containing severe pressure gradients in the neighborhood of shock waves or stag-

nation points, it proves necessary to augment the finite volume scheme by the addition of artificial dissipative terms. Therefore equation (4) is replaced by the equation

$$\frac{d}{dt}(hw) + Qw - Dw = 0 \tag{8}$$

where Q is the spatial discretization operator defined by equations (5-7), and D is a dissipative operator. Extensive numerical experiments have established that an effective form for Dw is a blend of second and fourth differences with coefficients which depend on the local pressure gradient.

The construction of the dissipative terms for each of the four dependent variables is similar. For the density equation

$$Dp = D_x\rho + D_Y P \tag{9}$$

where $D\rho$ and $D_Y\rho$ are corresponding contributions for the two coordinate directions, written in conservation form

$$D_x\rho = d_{i+\frac{1}{2},j} - d_{i-\frac{1}{2},j} \tag{10}$$

$$D_y\rho = d_{i,j+\frac{1}{2}} - d_{i,j-\frac{1}{2}}$$

The terms on the fight all have a similar form: for example

$$d_{i+\frac{1}{2},j} = \frac{h_{i+\frac{1}{2},j}}{\Delta t}\left\{\begin{array}{l}\varepsilon^{(2)}_{i+\frac{1}{2},j}\left(\rho_{i+1,j} - \rho_{i,j}\right) \\ -\varepsilon^{(4)}_{i+\frac{1}{2},j}\left(\rho_{i+2,j} - 3\rho_{i+1,j}\right. \\ \left. +3\rho_{i,j} - \rho_{i-1,j}\right)\end{array}\right\} \tag{11}$$

where h is the cell volume, and the coefficients $\varepsilon^{(2)}$ and $\varepsilon^{(4)}$ are adapted to the flow. Define

$$\nu_{i,j} = \frac{|p_{i+1,j} - 2p_{i,j} + p_{i-1,j}|}{|p_{i+1,j}| + 2|p_{i,j}| + |p_{i-1,j}|} \tag{12}$$

Then

$$\varepsilon^{(2)}_{i+\frac{1}{2},j} = \kappa^{(2)} \max\left(\nu_{i+1,j}, \nu_{i,j}\right) \tag{13}$$

and

$$\varepsilon^{(4)}_{i+\frac{1}{2},j} = \max\left(0, \left(\kappa^{(4)} - \varepsilon^{(2)}_{i+\frac{1}{2},j}\right)\right) \tag{14}$$

where typical values of the constants $\kappa^{(2)}$ and $\kappa^{(4)}$ are

$$\kappa^{(2)} = \frac{1}{4}, \quad \kappa^{(4)} = \frac{1}{256}$$

The dissipative terms for the remaining equations are obtained by substituting ρu, ρv and either ρE or ρH for ρ in these formulas.

The scaling $h/\Delta t$ in equation (11) conforms to the inclusion of the cell area h in the dependent variables of equation (8). Since equation (11) contains undivided differences, it follows that if $\varepsilon^{(2)} = O(\Delta x^2)$ and $\varepsilon^{(4)} = O(1)$, then, the added terms are of order Δx^3. This will be the case in a region where the flow is smooth. Near a shock wave $\varepsilon^{(2)} = O(1)$, and the scheme behaves locally like a first order accurate scheme.

It has been found that in smooth regions of the flow, the scheme is not sufficiently dissipative unless the fourth differences are included, with the result that calculations will generally not converge to a completely steady state. Instead, after they have reached an almost steady state, oscillations of *very* low amplitude continue indefinitely (with max $\frac{\partial \rho}{\partial t} \sim 10^3$, for example). These appear to be induced by reflections from the boundaries of the computational domain. Near shock waves it has been found that the fourth differences tend to induce overshoots, and therefore they are switched off by subtracting $\varepsilon^{(2)}$ from $\kappa^{(4)}$ in equation (14).

4. Time Stepping Schemes

Stable time stepping methods for equation (8) can be patterned on standard schemes for ordinary differential equations. Multistage two level schemes of the Runge Kutta type have the advantage that they do not require any special starting procedure, in contrast to leap frog and Adams Bashforth methods, for example. The extra stages can be used either

(1) to improve accuracy, or

(2) to extend the stability region.

An advantage of this approach is that the properties of these schemes have been widely investigated, and are readily available in textbooks on ordinary differential equations.

Consider a linear system of equations

$$\frac{dw}{dt} + Aw = 0.$$

Suppose that A can be expressed as $A=T\Lambda T^{-1}$ where T is the matrix of the eigenvectors of A, and Λ is diagonal. Then setting $v = T^{-1}w$ yields separate equations

$$\frac{dv_k}{dt} + \lambda_k v_k = 0$$

for each dependent variable v_k. The stability region is that region of the complex plane containing values of $\lambda\Delta t$ for which the scheme is stable. Consider now the model problem

$$\frac{\partial u}{\partial t} + a\frac{\partial u}{\partial x} + \varepsilon\Delta x\frac{\partial^2 u}{\partial x^2} = 0 \tag{15}$$

on a uniform mesh with interval Δx, with a dissipative term of order Δx. This can be reduced to a system or ordinary differential equations by introducing central-difference approximations for $\frac{\partial}{\partial x}$ and $\frac{\partial^2}{\partial x^2}$:

$$\frac{du_i}{dt} + \frac{a}{\Delta x}\left(u_{i+1} - u_{i-1}\right) + \frac{\varepsilon}{\Delta x}\left(u_{i+1} - 2u_i - u_{i-1}\right) = 0$$

Taking the Fourier transform in space

$$\hat{u} = \frac{1}{2\pi}\int_{-\infty}^{\infty} u e^{i\omega x} dx$$

this becomes

$$\frac{d\hat{u}}{dt} + \lambda\hat{u} = 0$$

where

$$\lambda = \frac{1}{\Delta x}\left(i\, a \sin \omega\Delta x - 4\varepsilon \sin^2 \frac{\omega\Delta x}{2}\right)$$

It can be seen that the maximum allowable value of the imaginary part of $\lambda\Delta t$ determines the maximum value of the Courant number $\frac{a\Delta t}{\Delta x}$ for which the calculation will be stable, while the addition of the dissipative term shifts the region of interest to the left of the imaginary axis.

In the present case, if the grid is held fixed in time so that tne cell area h is constant, the system of equations (8) has the form

$$\frac{dw}{dt} + Pw = 0 \qquad (16)$$

where if Q is the discretization operator defined in Section 2, and D is the dissipative operator defined in Section 3, the nonlinear operator P is defined as

$$Pw \equiv \frac{1}{h}(Qw - Dw) \qquad (17)$$

The investigation has concentrated on two time stepping schemes. The first is a three stage scheme which is defined as follows. Let a superscript n denote the time level, and let At be the time step. Then at time level n set

$$\begin{aligned} w^{(0)} &= w^n \\ w^{(1)} &= w^{(0)} - \Delta t\, Pw^{(0)} \\ w^{(2)} &= w^{(0)} - \frac{\Delta t}{2}\left(Pw^{(0)} + Pw^{(1)}\right) \\ w^{(3)} &= w^{(0)} - \frac{\Delta t}{2}\left(Pw^{(0)} + Pw^{(2)}\right) \\ w^{n+1} &= w^{(3)} \end{aligned} \qquad (18)$$

Variations of this scheme have been proposed by Gary[5], Stetter[6], and Graves and Johnson[10]. It can be regarded as a Crank Nicolson scheme with a fixed point iteration to determine the solution at time level n+1, and the iterations terminated after the third iteration. It is second order accurate in time, and for the model problem (15) with $\varepsilon=0$, it is stable when the Courant number

$$\left|\frac{a\Delta t}{\Delta x}\right| \leq 2$$

This bound is not increased by additional iterations. Compared uith standard third order Runge Kutta schemes, this scheme gives up third order accuracy in time for a larger bound on the Courant number.

The other scheme which has been extensively investigated is the classical fourth order Runge Kutta scheme, defined as follows. At time level n set

$$\begin{aligned} w^{(0)} &= w^n \\ w^{(1)} &= w^{(0)} - \frac{\Delta t}{2} Pw^{(0)} \\ w^{(2)} &= w^{(0)} - \frac{\Delta t}{2} Pw^{(1)} \\ w^{(3)} &= w^{(0)} - \Delta t\, Pw^{(2)} \\ w^{(4)} &= w^{(0)} - \frac{\Delta t}{6}\left(Pw^{(0)} + 2Pw^{(1)} + 2Pw^{(2)} + Pw^{(3)}\right) \\ w^{n+1} &= w^{(4)} \end{aligned} \qquad (19)$$

This scheme is fourth order accurate in time, and for the model problem (15) with $\varepsilon=0$, it is stable for Courant numbers

$$\left|\frac{a\Delta t}{\Delta x}\right| \leq 2\sqrt{2}$$

Its stability region, which is displayed on page 176 of Ref. (11), for example, also extends well to the left of the imaginary axis, alloxing latitude in the introduction of dissipative terms.

Both schenes have the property that if $Pw^n=0$ then $w^{(1)}=w^{(0)}$, and so on, so that $w^{n+1}=w^n$, and the steady state solution is

$$Pw = 0$$

independent of the time step At. This allows a variable time step determined by the bound on the local Courant number to be used to accelerate convergence to a steady state without altering the steady state.

The expense of re-evaluating the dissipative terms at every stage of these schemes is substantial. One method of avoiding this is to introduce the dissipative terns in a separate fractional step after the last stage of the Runge Kutta scheme. Then equation (17) is replaced by

$$Pw \equiv \frac{1}{h} Qw \qquad (17^*)$$

and the fourth order Runge Kurta scheme defined by equation (19). for example, is modified by setting

$$w^{n+1} = w^{(4)} + \Delta t D\, w^{(4)}$$

This method has the advantage that the stability properties for the two fractional steps are independent, so that the scheme will be stable if each fractional step is stable. It has the disadvantage that the steady state solution is no longer independent of the time step.

An alternative approach which has proved successful in practice, is to frcere the dissipatire terms at their values in the first stage. Thus the fourth order Runge Kurta scheme is modified so that it has ?he form

$$
\begin{aligned}
w^{(0)} &= w^n \\
w^{(1)} &= w^{(0)} - \frac{\Delta t}{2h} Qw^{(0)} + \frac{\Delta t}{2h} Dw^{(0)} \\
w^{(2)} &= w^{(0)} - \frac{\Delta t}{2h} Qw^{(1)} + \frac{\Delta t}{2h} Dw^{(0)} \\
w^{(3)} &= w^{(0)} - \frac{\Delta t}{h} Qw^{(2)} + \frac{\Delta t}{h} Dw^{(0)} \\
w^{(4)} &= w^{(0)} - \frac{\Delta t}{6h} (Qw^{(0)} + 2Qw^{(1)} + 2Qw^{(2)} + Qw^{(3)}) \\
&\quad + \frac{\Delta t}{h} Dw
\end{aligned}
\tag{20}
$$

The operators Q and D require roughly equal amounts of computation. Assigning to each 1 unit of work, and assuming that dissipative terms would be required in the leap frog or MacCormack schemes, both of which have maximum time steps bounded by a Courant number of one, one obtains the following table for the relative efficiency of the schenes:

Scheme	Evaluations of Q	Evaluations of D	Work	Maximum Courant Number	Efficiency = time step / work
Leap frog	1	1	2	1	1/2
MacCormack	2	1	3	1	1/3
3 stage	3	3	6	2	1/3
4 stage	4	4	8	2.8	.35
4 stage	4	1	5	2.8	.56

(frozen Dw)

5. Boundary Conditions

Improper treatment of the boundary conditions can lead to serious errors and perhaps instability. In order to treat the flow exterior to a profile one must introduce an artificial outer boundary to produce a bounded domain. If the flow is subsonic at infinity there will be three incoming characteristics where there is inflow across the boundary, and one outgoing characteristic, corresponding to the possibility of escaping acoustic waves. Where there is outflow, on the other hand, there will be three outgoing characteristics and one incoming characteristic. According to the theory of Kreiss[12], three conditions may therefore be specified at inflow, and one at outflow, while the remaining conditions are determined by the solution of the differential equation. It is not correct to specify free stream conditions at the outer boundary.

For the formulation of the boundary conditions it is convenient to assume a local transformation to coordinates X and Y such that the boundary coincides with a line Y = constant. Using subscripts X and Y to denote derivatives, the Jacobian

$$
h = x_X y_Y - x_Y y_X \tag{21}
$$

corresponds to the cell area of the finite volume scheme. Introduce the transformed flux vectors

$$
F = y_Y f - x_Y g \quad , \quad G = x_X g - y_X f \tag{22}
$$

where f and g are defined by equation (3). In differential form equation (2) then becomes

$$
\frac{\partial}{\partial t}(hw) + \frac{\partial F}{\partial X} + \frac{\partial G}{\partial Y} = 0 \tag{23}
$$

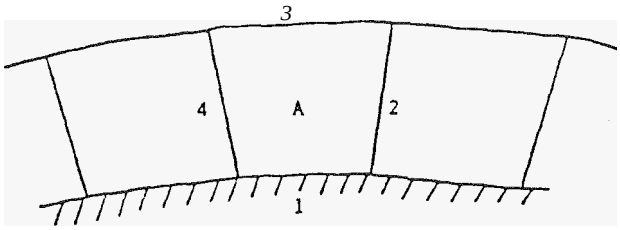

Consider first the boundary condition at the profile. Across side 1 of cell A in the sketch there is no convected flux since

$$
x_X v - y_X u = 0 \, . \tag{24}
$$

But there are contributions $\Delta y p$ and $\Delta x p$ to the momentum equations, which require an estimate of the pressure at the wall. Taking the time derivative of equation (24) multiplied by ρ, and substituting for $\frac{\partial}{\partial t}(h\rho u)$ and $\frac{\partial}{\partial t}(h\rho v)$ from equation (23) leads to the relation (given by Rizzi[13])

$$
(x_X^2 + y_X^2) p_Y = (x_X x_Y + y_X y_Y) p_X + \rho (y_Y u - x_Y v)(v x_{XX} + u y_{XX}) \tag{25}
$$

Thus we can estimate p_Y in terms of quantities which can be determined from the interior solution, and we can use this value of p_Y to extrapolate the pressure from the adjacent cell center to the wall.

Stable boundary conditions have been given by Gottlieb and Turkel[14] and Gustafsson and Oliger[15] for a variety of difference schemes. The treatment of the outer boundary condition adopted here follows similar lines. The equations are linearized about values at the end of the previous time step, and the characteristic variables corresponding to outgoing characteristics are then determined by extrapolation from the interior, while the remaining boundary conditions are specified in a manner consistent with the conditions imposed by the free stream. Let

$$
A = \frac{\partial F}{\partial w} \quad , \quad B = \frac{\partial G}{\partial w}
$$

Since the boundary is a line Y=constant, the eigenvalues of B determine the incoming and outgoing Characteristics. If q_n and q_t are the velocity components normal and tangential to the boundary, and c is the speed of sound, these eigenvalues are q_n, q_t, $q_n - c$, and $q_n + c$. Let values at the end of the previous time step be denoted by the subscript o, and let T_o be the eigenvector matrix of B_o. Then B_o is reduced to diagonal form by the transformation $A\Theta = T_o^{-1} B_o T_o$, and setting $v = T_o^{-1} w$, the linearized equation assumes the form

$$
\frac{\partial}{\partial t}(hv) + T_o^{-1} A_o T_o \frac{\partial v}{\partial X} + \Lambda_o \frac{\partial v}{\partial Y} = 0
$$

The characteristic variables are the components of V. These are $p-c_o^2\rho$, q_t, $p-\rho_o c_o q_n$ and $p_o+\rho_o c_o q_n$.

Let values extrapolated from the interior and free stream values be denoted by the subscripts e and ∞. Then at the inflow boundary we set

$$p - c^2\rho = p_\infty - c_o^2\rho_\infty \tag{26a}$$

$$q_t = q_{t_\infty} \tag{26b}$$

$$P - \rho_o c_o q_n = p_\infty - \rho_o c_o q_{n_\infty} \tag{26c}$$

$$P + \rho_o c_o q_n = p_e + \rho_o c_o q_{n_e} \tag{26d}$$

yielding

$$P = \frac{1}{2}\left(p_e + p_\infty - \rho_o c_o (q_{n_e} - q_{n_\infty})\right)$$

$$q_n = q_{n_\infty} + \frac{P-P_\infty}{\rho_o c_o}$$

The density can be determined from (26a). For steady state calculations it can alternatively be determined by specifying that the total enthalpy H has its free stream value.

At the outflow boundary one condition should be specified. If the flow is a parallel stream then $\frac{\partial p}{\partial y} = 0$, so for an open domain

$$P = p_\infty \tag{27}$$

A non reflecting boundary condition which would eliminate incoming waves is

$$\frac{\partial}{\partial t}(p-\rho_o c_o q_n) = 0 \tag{28}$$

This does not assure (27). Follosing Rudy and Strikwerda[16], (27) and (28) are therefore combined as

$$\frac{\partial}{\partial t}(p-\rho_o c_o q_n) + a(p-p_\infty) = 0 \tag{29}$$

where a typical value of the parameter a is 1/8. The velocity components and energy are extrapolated from the interior.

Various other boundary conditions designed to reduce reflections from the outer boundary have been proposed by several authors[17,18], and it seems that it would be worth while to test some of these alternatives.

6. Convergence Acceleration

Two devices have been used to accelerate the convergence of the solutions to a steady state. The first is to use the largest possible time step permitted by the local stability bound everywhere in the computational domain. This has the effect of assuring that disturbances are propogated the whole way across the domain in a number of time steps of the same order as the number of mesh intervals. It can be regarded as scaling the wave speed to give equations of the form

$$\frac{\partial w}{\partial t} + \lambda\left(\frac{\partial f}{\partial x} + \frac{\partial g}{\partial y}\right) = 0$$

where λ is proportional to the local mesh interval. Assuming that a stretched grid is used to extend the computational domain away from the profile, λ will be very large near the outer edge of the domain.

As a model for this procedure consider the wave equation in polar coordinates r and θ,

$$\phi_{tt} = c^2\left(\frac{1}{r}\frac{\partial}{\partial r}(r\phi_r) + \frac{1}{r^2}\phi_{\theta\theta}\right)$$

Suppose that the wave speed c is proportional to the radius, say $c = \alpha r$. Then

$$\phi_{tt} = \alpha^2\left(r\frac{\partial}{\partial r}(r\phi_r) + \phi_{\theta\theta}\right)$$

This has solutions of the form

$$\phi = \frac{1}{r^n} e^{-\alpha n t}$$

suggesting the possibi1ity of exponential decay.

A more sophisticated modification of the equations, which is presently being investigated, is to set

$$\frac{\partial w}{\partial t} + M\left(\frac{\partial f}{\partial x} + \frac{\partial g}{\partial y}\right) = 0$$

where the matrix M couples the equations for ρ, ρu, ρv and ρE, and modifies the eigenvalues of the system.

The second device for convergence acceleration is to introduce a forcing term proportional to the difference between the total enthalpy H and its free stream value H_∞. In a steady flos with a uniform free stream $H=H_\infty$ throughout the domain. The density and energy equations

$$\frac{\partial}{\partial x}(\rho u) + \frac{\partial}{\partial y}(\rho v) = 0$$

and

$$\frac{\partial}{\partial x}(\rho u H) + \frac{\partial}{\partial y}(\rho v H) = 0$$

are then consistent. This property is not preserved by various predictor corrector difference schemes, such as the MacCormack scheme. It is preserved by the schemes defined in sections 2-4, however, provided that the dissipative operator is applied to ρH and not ρE in the energy equation. Thus a forcing term proportional to $H-H_\infty$ does not alter the steady state.

The reason for introducing such a term is to provide additional damping, The term is intended to have an effecr similar to that of the term containing ϕ_t in the telegraph equation:

$$\phi_{tt} + \alpha \phi_t = \phi_{xx} + \phi_{yy}$$

Multiplying this equation by ϕ_t, and integrating by parts over all space leads to the relation

$$\frac{\partial P}{\partial t} + \alpha \int_{-\infty}^{\infty}\int_{-\infty}^{\infty} \phi_t^2 \, dxdy = 0$$

where

$$P = \frac{1}{2} \int_{-\infty}^{\infty}\int_{-\infty}^{\infty} (\phi_t^2 + \phi_x^2 + \phi_y^2) \, dxdy$$

Since P is non negative, it must decay if $\alpha > 0$ until $\phi = 0$. When relaxarion methods are regarded as sirnufating time dependent equations, it is similarly found that the term containing ϕ_t plays a critical role in determining the rate of convergence[19].

In subsonic flow the Euler equations are equivalent to the unsteady potential flow equation

$$\phi_{tt} + 2u\phi_{xt} + 2v\phi_{yt} = (c^2-u^2)\phi_{xx} - 2uv\phi_{xy} + (c^2-v^2)\phi_{yy} \qquad (30)$$

which can be reduced to the wave equation by introducing moving coordinates $x' = x-ut$, $y' = y-vt$. Also rhe unsteady Bernoulli equation is

$$\phi_t + H = H_\infty$$

It can be verified that if the Euler equations are written in primitive form, and the density equation is modified by the addition of a term proportional to $H-H_\infty$, so that it becomes

$$\frac{\partial \rho}{\partial t} + u \frac{\partial \rho}{\partial x} + v \frac{\partial \rho}{\partial y} + \rho \left(\frac{\partial u}{\partial x} + \frac{\partial v}{\partial y}\right) + \alpha \rho (H-H_\infty) = 0$$

then the flow remains irrotational in the absence of shock waves, and equation (30) is modified by a term proportional to ϕ_t. When the density equation is combined with the momentum equations to yield a system of equations in conservation form, the modified equations become

$$\frac{\partial \rho}{\partial t} + \frac{\partial}{\partial x}(\rho u) + \frac{\partial}{\partial y}(\rho v) + \alpha \rho (H-H_\infty) = 0$$

$$\frac{\partial}{\partial t}(\rho u) + \frac{\partial}{\partial x}(\rho u^2 + p) + \frac{\partial}{\partial y}(\rho v u) + \alpha \rho u (H-H_\infty) = 0$$

$$\frac{\partial}{\partial t}(\rho v) + \frac{\partial}{\partial x}(\rho u v) + \frac{\partial}{\partial y}(\rho v^2 + p) + \alpha \rho v (H-H_\infty) = 0$$

$$\frac{\partial}{\partial t}(\rho E) + \frac{\partial}{\partial x}(\rho u H) + \frac{\partial}{\partial y}(\rho v H) + \alpha \rho H (H-H_\infty) = 0$$

The energy equation now has a quadratic term in H, like a Riccati equation. This can be destabilizing, and an alternative which has been found effective in practice is to modify the energy equation to the form

$$\frac{\partial}{\partial t}(\rho E) + \frac{\partial}{\partial x}(\rho u H) + \frac{\partial}{\partial y}(\rho v H) + \alpha (H-H_\infty) = 0$$

which tends to drive H towards H_∞. The additional terms can conveniently be introduced in a separate fractional step at the end of each time step.

7. Results

Some typical results of numerical calculations are presented in this section. Since the purpose is primarily to show the accuracy and convergence of the basic numerical algorithm, the examples are restricted to nonlifting flow past a cylinder and a NACA 0012 airfoil. Only the flow in the upper half plane was calculated, and an O mesh was used with 64 intervals in the chord wise direction and 32 intervals in the normal direction. The mesh extended to a distance of about 25 chords from the profile, and the mesh interval near the outer boundary was of the order of a chord. In the case of the NACA 0012 airfoil, the cells adjacent to the outer boundary had an area 2.5 million times greater than the area of the smallest cell, located at the trailing edge. Extensive numerical experiments confirmed the superior efficiency of the modified fourth order Runge Kutta scheme defined by equation (20), and this scheme was used to produce all the results displayed in this section.

Figure 1 shows results for flow past a circular cylinder. The grid is displayed in Figure 1(a). Figures 1(b) and 1(c) show the computed pressure distributions for Mach numbers of .35 and .45. The flow is fully subsonic in the first case, and there should be no departure from fore and aft symmetry in an exact calculation. The flow should also be isentropic. The calculations are normalized with $p=1$ and $\rho=1$ at infinity, so the quantity $S=p/\rho^\gamma - 1$ can be used as a measure of entropy generation. The largest computed value of S was .0003, at a point along the surface. At Mach .45 there is a moderately strong shock wave, as can be seen. The entropy was computed to be .0120 behind the shock wave. Figure 1(d) shows the convergence history for the flow at Mach .45. The measure of convergence is the residual for the density, defined as the root mean square value of $\frac{\partial \rho}{\partial t}$ (calculated as $\Delta\rho/\Delta t$ for the complete time step). This was reduced from 1.67 to $.486\ 10^{-3}$ in 1000 cycles. The mean rate of convergence was .978 per cycle. Another measure of convergence (not plotted) is the root mean square deviation of the total enthalpy from its free stream value. This was reduced from .0828 to $.500\ 10^{-3}$. Enthalpy damping was used in this calculation to accelerate convergence. The calculation was started impulsively by suddenly introducing the cylindrical obstacle into a uniform flow, and immediately enforcing the solid wall boundary condition at its surface. This creates very large disturbances, but the pattern of the flow field is still quite rapidly established. One measure of this is the size of the supersonic zone. In this case the number of supersonic points was frozen after 450 cycles.

Figure 2 shows a comparison between the results of potential flow and Euler calculations for a NACA 0012 airfoil at zero degrees angle of attack and Mach .850. The mesh is shown in Figure 2(a), the potential flow result is shown in Figure 2(b), and the Euler result is shown in Figure 2(c). It

can be seen that the shock wave is further aft in the potential flow calculation, which was performed by the fully conservative finite volume method of Jameson and Caughey[20], using a first order accurate formulation in the supersonic zone. The convergence history of the Euler calculation is shown in Figure 2(d). Figures 3(a) and 3(b) show a similar comparison between the potential flow and Euler results for the NACA 0012 airfoil at Mach .800. In this case the shock locations are identical. Figures 3(c) and 3(d) show the convergence history over 1500 cycles with and without enthalpy damping. Without enthalpy damping the final residual is $.269\ 10^{-6}$. With enthalpy damping it is $.240\ 10^{-9}$. These runs used the potential flow result as the starting condition for the Euler calculation. Thus the flow pattern was already essentially established at the start of the Euler calculation, with the result that the number of points in the supersonic zone was frozen after 180 cycles when enthalpy damping was used. To illustrate the development of the flow field without the assistance of the potential flow calculation, Figure 4 shows the result for the same flow after 200, 400, 600 and 800 cycles with an impulsive start. Finally a print out of the computed density, velocity components, total enthalpy, pressure, Mach number, and entropy (measured as $S > p/\rho^{\gamma}-1$) is displayed in Figure 5. In an exact calculation S would be zero upstream of the shock wave. Actually it has a value of -.0017 near the leading edge. Then it settles to values in the range of .0002 to .0009 ahead of the shock wave, and rises to .0054 behind the shock wave.

These results supporr the conclusions stated in the introduction. It also appears that shock waves can be satisfactorily captured without resorting to flux vector splitting and one sided differencing[21-24], at least for steady state calculations, and that fairly rapid convergence to a steady state can be obtained without the use of an implicit scheme.

Attractive features of the scheme are its comparative simplicity, and its susceptibility to the extensive use of vector operations on a vector computer. The present implementation of the fourth order Runge Kutta scheme requires 426 floating point operations at each interior cell. On a mesh with 64x32 = 2048 cells a single cycle therefore requires about .9 megaflops (million floating point operations). In tests on a Cray 1 computer it has been found that the program operates at 44 cycles per second (corresponding to a computing speed of about 40 megaflops per second). The code is written in standard FORTRAN, and this rate was achieved simply by relying on the capability of the Cray FORTRAN computer to vectorize the code automatically. A still higher rate could be realized by writing certain critical segments of the program in assembly language. In practice a typical run is more than sufficiently converged for engineering applications within 500 cycles. At 44 cycles a second such a calculation would be completed in 12 seconds, (or 24 seconds for a lifting case with twice as many mesh cells to represent the flow in both the upper or lower half planes, provided that the same rate of convergence could be realized).

8. Acknowledgements

This work was supported by the Office of Naval Research under Contract N00014-81-K-0379 and by NASA under Contract NAG2-96.

References

1. Jameson, A. "Numerical Calculation of Transonic Flow with Shock Waves". *Symposium Transsonicum II*, Gottingen, 1975, Springer-Verlag, 1976.

2. Rizzi, A., and Viviand, H. (editors), "Numerical Methods for the Computation of Inviscid Transonic Flow with Shocks", Proceedings of GAMM Workshop, Stockholm, 1979, Viewveg Verlag, 1981

3. Steinhoff, J. and Jameson, A. "Multiple Solutions of the Transonic Potential Flow Equation", Fifth AIAA Computational Fluid Dynamics Conference, Palo Alto, 1981.

4. Rizzi, A. "Computation of Rotational Transonic Flow, in Numerical Methods for the Computation of Inviscid Transonic Flow with Shocks", Proceedings of GAMM Workshop, *Stockholm, 1979, Viewveg Verlag, 1981.*

5. Gary, J. "On Certain Finite Difference Schemes for Hyperbolic Systems", Math. Comp., Vol. 18, pp. 1-18, 1964.

6. Stetter, H.J. "Improved Absolute Stability of Predictor-Corrector Schemes", Computing, Vol. 3, pp. 286-296, 1968.

7. Rizzi, A. and Eriksson, L.E. "Transfinite West Generation and Damped Euler Equation Algorithm for Transonic Flox Around Xing-body Configurations", Fifth AIAA Computational Fluid Dynamics Conference, Palo Alto, 1981.

8. Viviand, H. "Pseudo Unsteady Methods for Transonic Flow Computations", Proceedings of Seventh International Conference on Numerical Methods in Fluid Dynamics, Stanford, 1980, Springer-Verlag. 1981.

9. Jameson, A., Rizzi, A., Schmidt, W., and Whitfield, D. "Finite Volume Solution for the Euler Equation for Transonic Flow over Airfoils and Wings Including Viscous Effects", AIM Paper 81-1265, 1981.

10. Graves, R. and Johnson, N. "Navier Stokes Solutions Using Stetter's Method, AIM Journal, Vol. 16, pp. 1013-1015, 1978.

11. Stetter, H.J. "Analysis of Discreti-ation Merhods for Ordinary Differential Equations", Springer-Verlag. 1973.

12. Kreiss, H.O. "Initial Boundary Value Problems for Hyperbolic Systems", Comm. Pure Appl. Math., Vol. 23, pp. 217-290, 1970.

13. Rizzi, A. "Numerics1 Implementation of Solid Body Boundary Conditions for the Euler Equations", ZAMM Vol. *58*, pp. 301-304, 1978.

14. Goctlieb, D. and Turkel, E. "Boundary Conditions for Multistep Finite Difference Methods for Time Dependent Equations", J. Computational Physics, Vol. *26*, pp. 181-196, 1978.

15. Gustafsson, B. and Oliger, J. "Stable Boundary Approximations for a Class of Time Discreti-ations of $u_t = AD_0 u$", Upsala University, Dept. of Computer Sciences, Report 87, 1980.

16. Rudy, D. and Strikwerda, J. "A Non-reflecting Outflow Boundary Condition for Subsonic Navier Stokes Calculations", J. Computational Physics, Vol. 36, pp. 55-70, 1980.

17. Engquist, B. and Majda, A. "Absorbing Boundary Conditions for the Numerical Simulation of Waves", Math. Comp. Vol. 31, pp. 629-651, 1977.

18. Bayliss, A. and Turkel, E. "Outflow Boundary Conditions for Fluid Dynamics" ICASE Report 80-21, 1980.

19. Garabedian, P.R. "Estimation of the Relaxation Factor for Small Mesh Size", Math Tables Aids Comp., Vol. 10, pp. 183-185, 1956.

20. Caughey, D. and Jameson, A. "Basic Advances in the Finite Volume Method for Transonic Potential Flow Calculations", Symposium on Numerical and Physical Aspects of Aerodynamic Flows, Long Beach, 1981.

21. Steger, J. and Warming, R. "Flux Vector Splitting for the Inviscid Gas Dynamic Equations with Application to Finite Difference Methods". NASA TM 78605, 1979.

22. Roe, P.L. "The Use of the Riemann Problem in Finite Difference Schemes", Proceedings of Seventh International Conference on Numerical Methods in Fluid Dynamics, Stanford, 1980, Springer-Verlag, 1981.

23. Roe, P.L. "Numerical Algorithms for the Linear Wave Equation", Royal Aircraft Establishment Memorandum, 1980.

24. Van Leer, B. "Towards the Ultimate Conservative Differencing Scheme, V, A Second Order Sequel to Godunov's Method", J. Computational Physics, Vol. 32, pp. 101-126, 1979.

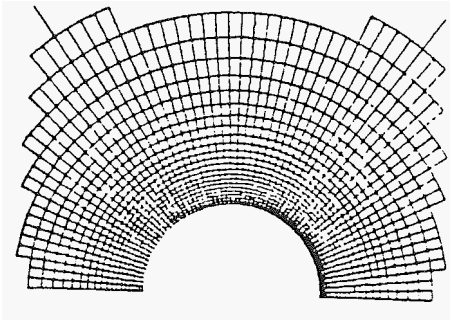

(a) Mesh

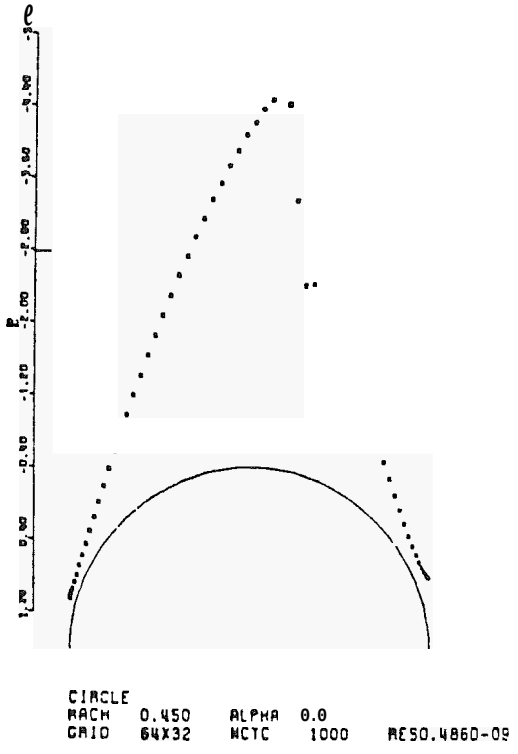

(c) Transonic flow

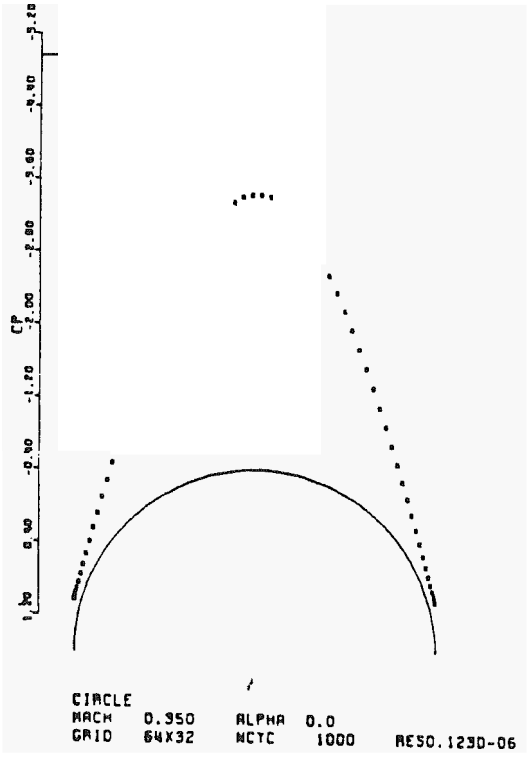

(b) Subsonic flow

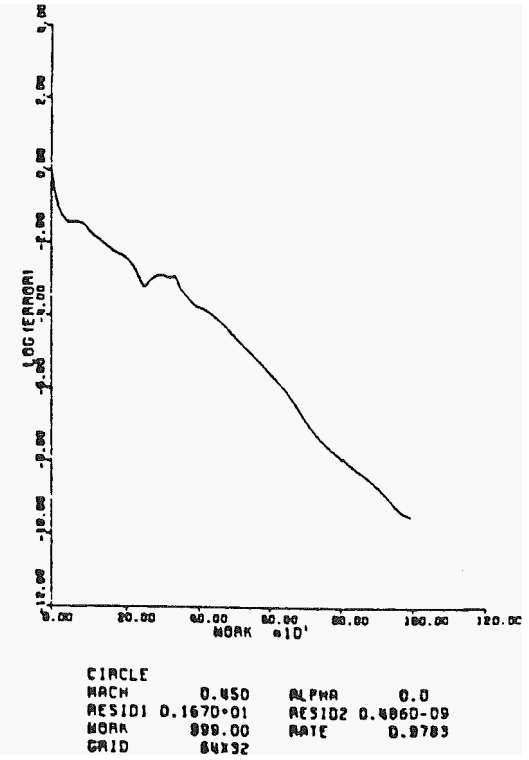

(d) Convergence history

Figure (1)

Flow past a circle.

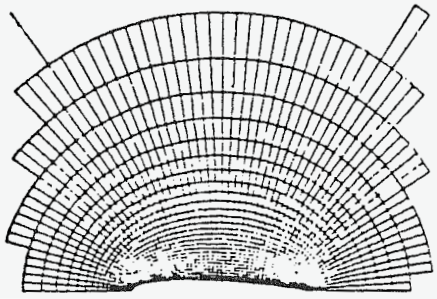

(a) Mesh

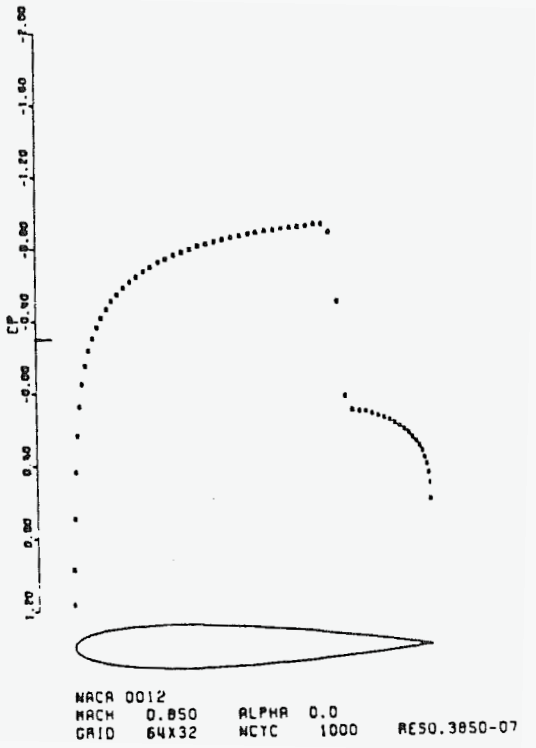

(c) Euler equations

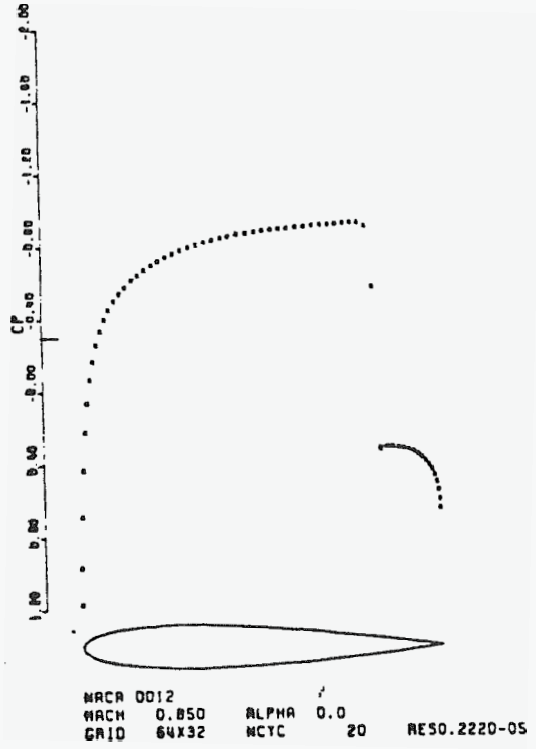

(b) Potential flow

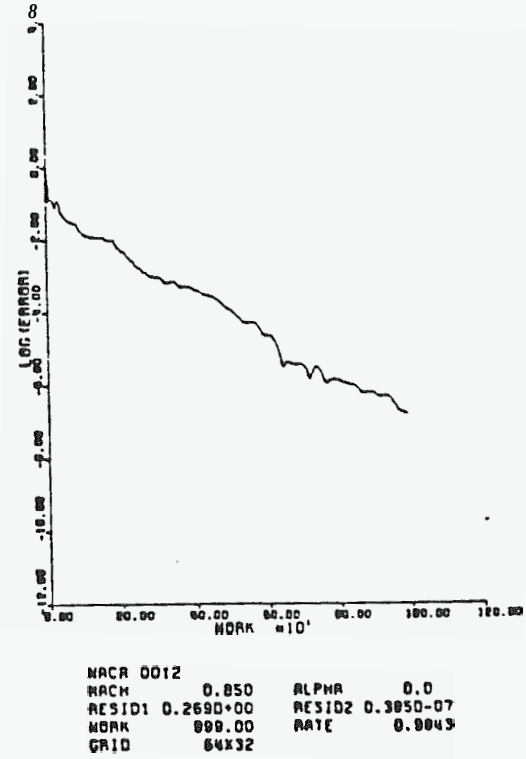

(d) Convergence history

Figure (2)

NACA 0012 airfoil at Mach .85

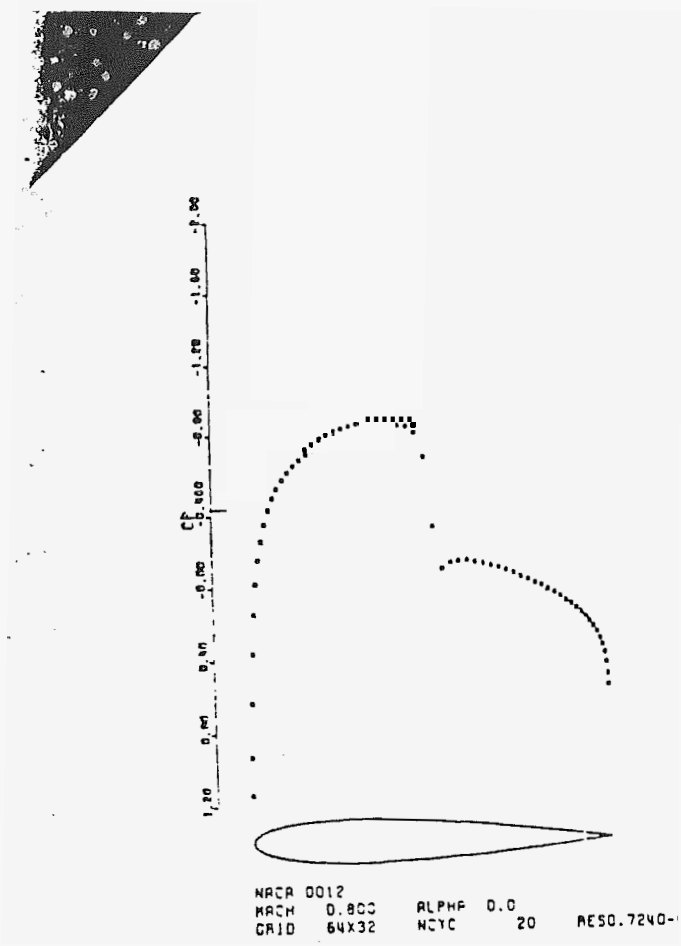

(a) Potential flow

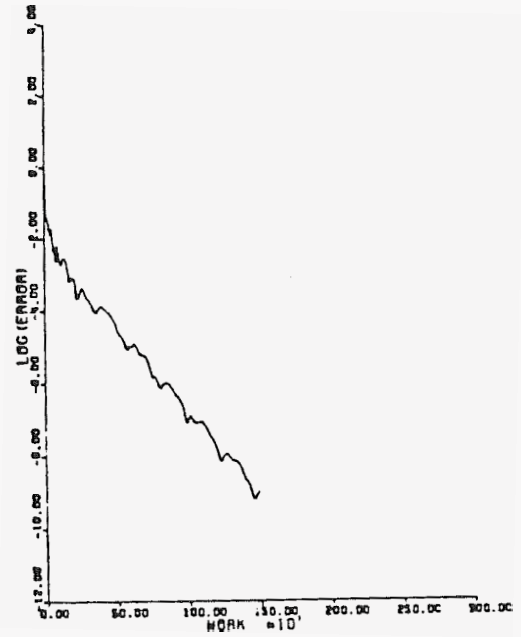

(c) Convergence with enthalpy damping

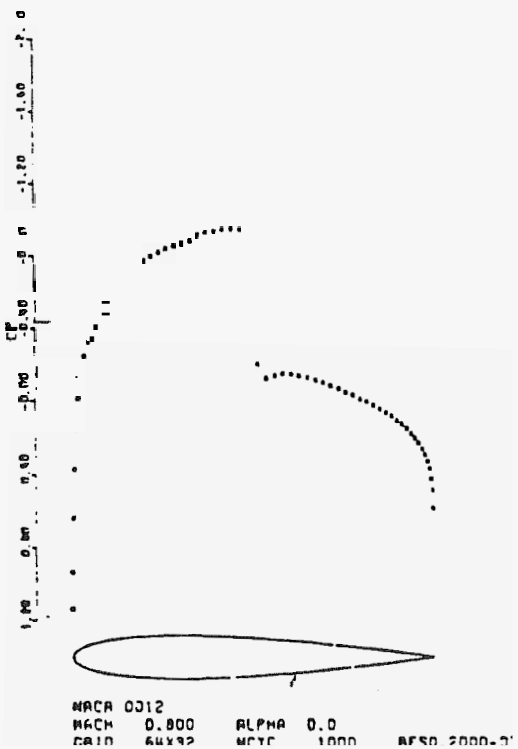

(b) Euler equations

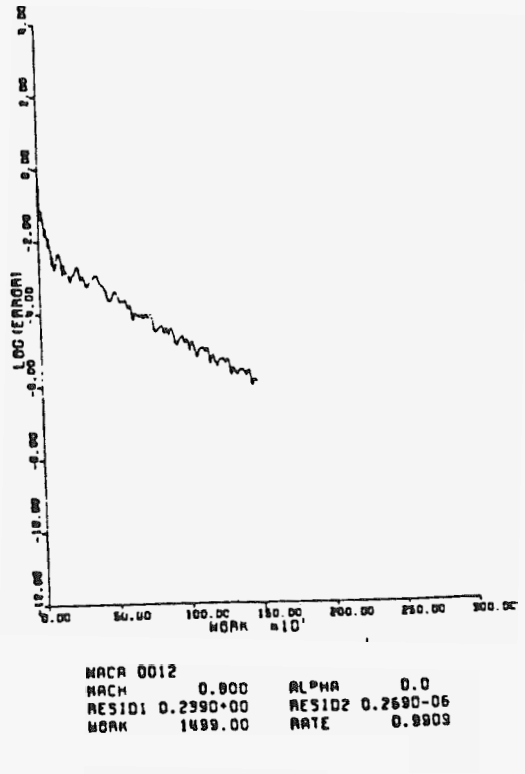

[d) Convergence without enthalpy d

Figure 3

NACA 0012 airfoil at Mach .80

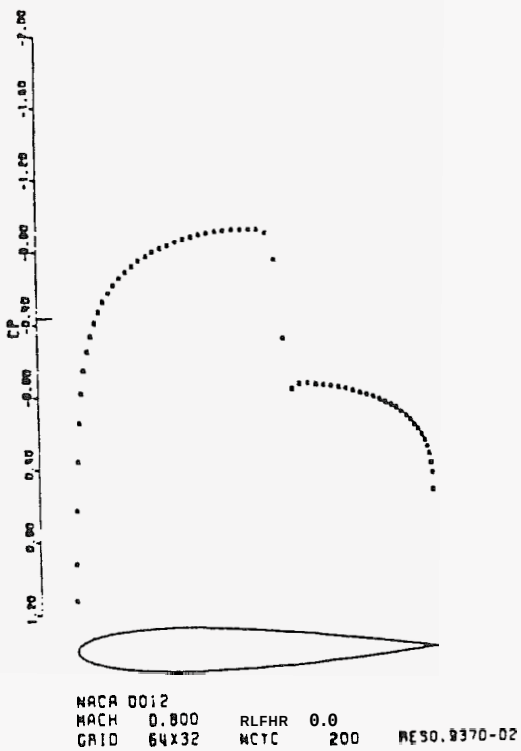

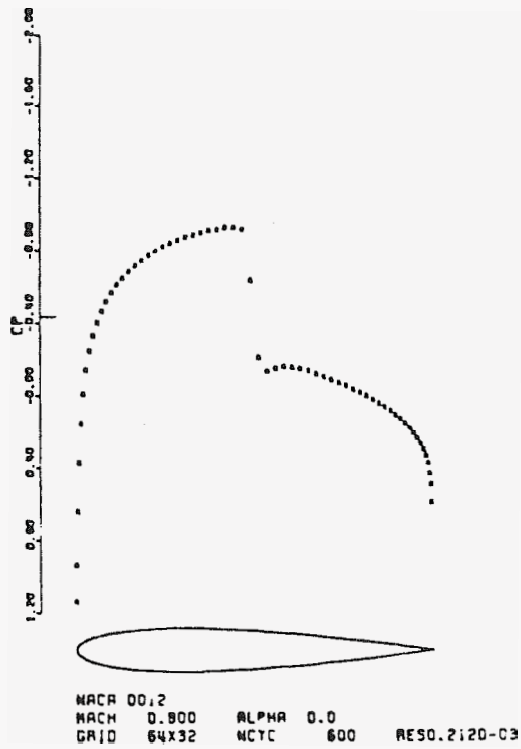

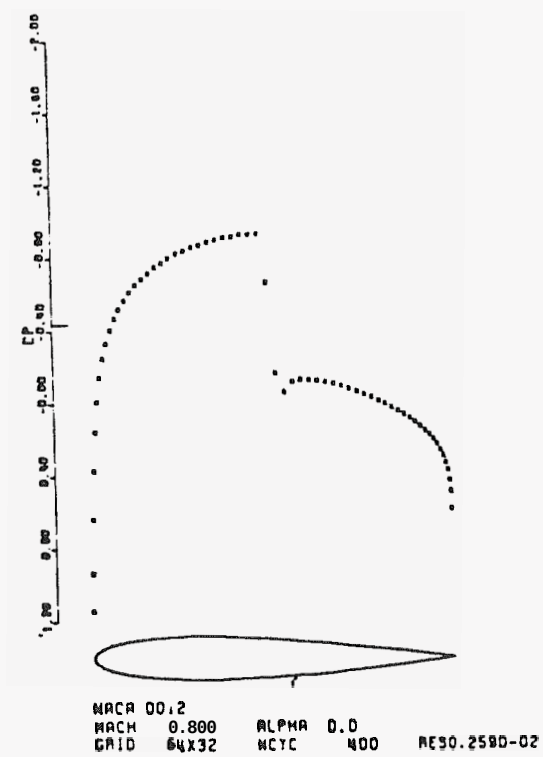

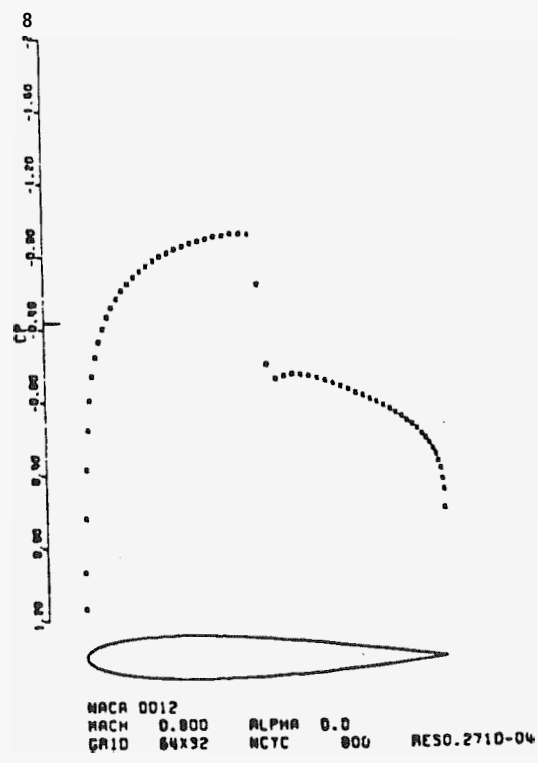

Figure (4)

Development of flow field: NACA 0012 airfoil at Mach .80

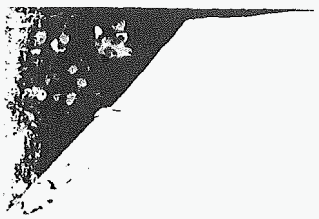

I	J	RHO	U	V	H	P	MACH	S
1	1	1.3433	0.0895	0.122;	0.0000	1.5109	0.1207	−0.0003
2	1	1.2950	0.2111	0.3198	0.0000	1.4336	0.3078	−0.0017
3	1	1.2160	0.3910	0.4296	0.0000	1.3130	0.4725	−0.0014
4	1	1.1369	0.5661	0.4645	0.0000	1.1953	0.6036	−0.0012
5	1	1.0695	0.7105	0.4552	0.0000	1.0976	0.7039	−0.0009
6	1	1.0240	0.8240	0.4264	0.0000	1.0192	0.7821	−0.0006
7	1	0.9893	0.0121	0.3906	0.0000	0.9570	0.8436	−0.0002
9	1	0.9328	0.9813	0.3538	0.0000	0.9072	0.8940	−0.0000
9	1	0.9025	1.0369	0.3182	0.0000	0.8663	0.9356	0.0001
10	1	0.8769	1.0825	0.2047	0.0000	0.8321	0.9711	0.0002
11	1	0.8547	1.1205	0.2537	0.6000	0.8030	1.0018	0.0003
12	1	0.8354	1.1528	0.2249	0.0000	0.7777	1.0289	0.0003
13	1	0.8181	1.1808	0.1982	0.0000	0.7553	1.0532	0.0004
14	1	0.8026	1.2054	0.1734	0.0000	0.7353	1.0753	0.000-1
15	1	0.7884	1.2269	0.1501	0.0000	0.7173	1.0953	0.0005
16	1	0.7758	1.2462	0.1284	0.0000	0.7011	1.1137	0.0004
17	1	0.7640	1.2632	0.1079	0.0000	0.6864	1.1304	0.0005
8	1	0.7535	1.2786	0.0887	0.0000	0.6731	1.146.	0.0004
19	1	0.7436	1.2920	0.0705	0.0000	0.6609	1.1600	0.0000
20	1	0.7351	1.3045	0.0535	0.0000	0.6501	1.1733	0.0004
21	1	0.7267	1.3151	0.0374	0.0000	0.6400	1.1846	0.0007
22	1	0.7199	1.3252	0.0222	0.0000	0.6313	1.196.	0.0003
23	1	0.7128	1.3333	0.0030	0.0000	0.6230	1.2053	0.0005
24	1	0.7075	1.3414	-0.0054	0.0000	0.6163	1.2142	0.0005
25	1	0.7015	1.3473	-0.0179	0.0000	0.6094	1.2219	0.0009
26	1	0.6780	1.3537	-0.0298	0.0000	0.6046	1.2200	0.0000
27	1	0.6930	1.3575	−0.0406	0.0000	0.5991	1.2344	0.0011
28	1	0.6897	1.3613	-0.0512	0.0000	0.5969	1.2354	-0.0000
29	1	0.6871	1.3642	−0.0603	0.0000	0.5920	1.2434	0.0012
30	1	0.6866	1.3677	−0.0697	0.0000	0.5905	1.248.	-0.0004
31	1	0.6869	1.3619	−0.0771	0.0000	0.5922	1.2416	0.0020
32	1	0.7012	1.2238	-0.0771	0.0000	0.7134	1.0845	0.0060
33	1	0.9187	1.0204	-0.0710	0.0000	0.9087	0.8739	0.0079
34	1	0.9280	0.9872	-0.0722	0.0000	0.9466	0.8416	0.0052
35	1	0.9325	0.9945	−0.0763	0.0000	0.9391	0.8490	0.0052
36	1	0.9485	0.9994	-0.0805	0.0000	0.9337	0.8543	0.0054
37	1	0.9495	0.9976	−0.0640	-0.0000	0.9356	0.8526	0.0054
38	1	0.9527	0.9929	-0.0870	−0.0000	0.9354	0.8463	0.0054
39	1	0.9564	0.9871	−0.0898	-0.0000	0.9446	0.8430	0.0054
40	1	0.9607	0.9807	−0.0923	−0.0000	0.9505	0.8369	0.0054
41	1	0.9654	0.9734	−0.0946	-0.0000	0.9574	0.8304	0.0054
42	1	0.9706	0.9656	−0.0966	−0.0000	0.9646	0.8229	0.0054
43	1	0.9759	0.9575	−0.0984	−0.0000	0.9747	0.8153	0.0054
44	1	0.9815	0.9490	-0.1001	-0.0000	0.9794	0.8074	0.0054
45	1	0.9871	0.9403	-0.1016	-0.0000	0.9874	0.7992	0.0054
46	1	0.9930	0.9313	-0.1030	-0.0000	0.9955	0.7903	0.0055
47	1	0.9989	0.9221	-0.1042	-0.0000	1.0039	0.7824	0.0054
48	1	1.0050	0.9127	-0.1054	-0.0000	1.0125	0.7736	0.0054
49	1	1.0113	0.9029	-0.1063	-0.0000	1.0213	0.7645	0.0054
50	1	1.0177	0.8928	-0.1071	-0.0000	1.0304	0.7552	0.0054
51	1	1.0243	0.8823	-0.1077	-0.0000	1.0398	0.7456	0.0054
52	1	1.0312	0.8715	-0.108	−0.0000	1.0496	0.7357	0.0054
53	1	1.0382	0.8602	-0.1084	-0.0000	1.0596	0.7253	0.0054
54	1	1.0456	0.8483	-0.1085	−0.0000	1.0702	0.7144	0.0054
55	1	1.0533	0.8357	−0.1082	-0.0000	1.0813	0.7029	0.0054
56	1	1.0615	0.8225	-0.1077	-0.0000	1.0931	0.6909	0.0054
57	1	1.0701	0.8082	-0.1069	-0.0000	1.1054	0.6779	0.0054
58	1	1.0795	0.7928	-0.1058	-0.0000	1.1190	0.6639	0.0054
59	1	1.0895	0.7756	-0.1039	-0.0006	1.1336	0.6484	0.0055
60	1	1.1012	0.7564	-0.1015	-0.0000	1.1505	0.6310	0.0053
61	1	1.1136	0.7336	-0.0993	-0.0000	1.1689	0.6105	0.0055
62	1	1.1306	0.7063	-0.0927	-0.0000	1.1933	0.5860	0.0049
63	1	1.1489	0.6660	-0.0858	-0.0000	1.2220	0.5503	0.0046
64	1	1.1683	0.6133	-0.0667	-0.0000	1.2683	0.5032	0.0044
65	1	1.1813	0.6133	0.0667	-0.0000	1.2683	0.5032	0.0044

Figure (5)
Printout of flow field quantities in the cells along the surface
NACA 0012 airfoil at Mach .80